文章编号 2095-1531(2018)02-0237-11

# Finite element analysis of infrared thermal imaging for four-layers structure of human thigh

LIU Hong-yan[1,2], SUN Qiang[1,2*]
(1. *Changchun Institute of Optics, Fine Mechanics and Physics, Chinese Academy of Sciences, Changchun* 130033, *China*;
2. *University of Chinese Academy of Sciences, Beijing* 100049, *China*)
* *Corresponding author, E-mail: sunq@ciomp.ac.cn*

**Abstract:** To investigate the relevancy of infrared thermal imaging and tumors inside human body, the finite element model of human thigh with four-layers, including bone, muscle, fat and skin layers, is established in this paper. Based on the characteristic that temperature varies along radial direction inside the body, the heat generation rate of blood perfusion as a function of polar radius in each layer is given. By this method the non-linear problem of temperature-dependence of the heat generation rate of blood perfusion in finite element analysis is solved. Then the temperature distributions caused by the inside tumor with different sizes and at different depths are numerically calculated by finite element analysis. It can be concluded that in the given range of tumor diameters a smaller tumor yields larger temperature increases inside the body, higher peak temperature and narrower FWHM(Full Width at Half Maximum) of the temperature distribution on the skin surface. It is also shown that with specific diameter, tumors located deeper yield higher peak temperature inside the body, and lower peak temperature and wider FWHM on the skin surface.

**Key words:** finite element analysis(FEA); infrared optics; heat transfer analysis; infrared medical imaging

# 人体腿部四层结构的红外热成像有限元分析

刘宏岩[1,2], 孙 强[1,2*]
(1. 中国科学院 长春光学精密机械与物理研究所, 吉林 长春 100033;
2. 中国科学院大学, 北京 100049)

**摘要:** 为研究人体红外热成像和体内肿瘤热源的关联, 本文构建了包括骨层、肌肉层、脂肪层、皮肤层的人体腿部有限元模型。根据体内温度沿径向分布的特点, 给出了各区域内动脉血液灌注热生成率随径向坐标变化的情况, 解决了有限元建模中动脉血灌注热生成率随温度变化的非线性问题。进而用有限元方法数值计算了不同尺寸和不同深度的体内肿瘤所带来的温度变化。结果表明: 在所研究的肿瘤尺寸范围内, 肿瘤尺寸越小, 体内温度提升越高, 体表的峰值温度越高,

**收稿日期:** 2017-11-08; **修订日期:** 2018-01-13

体表温度分布半峰宽越窄，温度变化越陡峭。对于特定尺寸的肿瘤，肿瘤越深，体内峰值温度越高，体表的峰值温度越低，体表温度分布半峰宽越宽，温度变化越平缓。

关 键 词: 有限元分析; 红外光学; 热传导分析; 红外医学成像
中图分类号: O59 文献标识码: A doi: 10.3788/CO.20181102.0237

## 1 Introduction

Infrared imaging technology has been widely applied in the military and remote sensing fields. Recently it has also been paid close attention in biomedical field due to its characteristics of non-invasive diagnosis, risk-free of ionizing radiation and no inflicting pain on patients [1-3]. Furthermore, infrared thermal imaging diagnosis is specifically worthwhile during the early stage of tumor growth for its physiological test nature [4-5]. This is compared with X-ray or ultrasonic imaging diagnosis which relies on anatomical test only. Usually physiological change precedes anatomical change when one part of human body gets sick [6-7], and so the combination of X-ray imaging with infrared thermal imaging can improve the sensitivity of tumor detection greatly especially at early stage [8-10].

The radiation of skin surface is approximate to that of blackbody with the peak value at about 9.4 μm and the spectral emissivity between 0.98 and 1.0. The total radiation emission of blackbody increases rapidly as the temperature increases. The infrared thermal camera collects the radiation energy of skin surface along the camera direction. Then the temperature distribution on the skin surface is obtained according to the collected radiation energy, the object distance and the radiation direction, by suitable computation and calibration. Infrared thermal image is a two-dimensional map of temperature on skin surface which the size and position of tumor inside the body cannot be acquired directly. In 1948, Pennes established the differential equation of the heat transfer in biological tissues to calculate the temperature distribution inside the body [11]. However, the human body is of multiple layers with different thermo-physical parameters for each layer and analytical solutions of Pennes´ bio-heat transfer equation cannot be obtained normally. Therefore numerical methodology based on human anatomy and finite element analysis becomes the main means of studying heat conduction in human body. Furthermore, as for the topic of inverse heat transfer, forming a more realistic direct model and giving the direct solutions under various heat sources are of significance [12-13].

M. S. Ferreira *et al*. established a three-dimensional model of human body composed of 15 cylindrical elements, and numerically studied the heat transfer between large arteries and veins [14]. K. R. Pardasani *et al*. developed a finite element model using two-dimensional coaxial circular sector elements to study radial and angular heat distribution in dermal regions of human limbs [15]. M. Agrawal *et al*. developed a finite element model of human limbs with the geometry of elliptical tapered shape, and computed to obtain tissue temperature distributions with different parameters like atmospheric temperature, evaporation rate and thickness of tissues [16]. R. Hatwar *et al*. considered the multilayer´s tissue structure and the variation of tumor´s size and depth, and then developed a multilayered finite element model of human body [17].

Domestically, G. L. Shi *et al*. acquired firstly the q-r characteristic curve of heat intensity varying with depth which was then used as a criteria of diseases clinically [3]. The diagnosis results of four typical clinical practices were consistent with those of X-ray and B-ultrasonic. C. Y. Wang *et al*. investigated the relationship between the information of the heat source and the surface temperature distribution by building a two-dimensional finite element analysis model [18]. Simulation results were validated by

physical experiments with adjustable heat source buried in layered biological tissues. H. Q. Yang *et al.* constructed a multi-dimensional model of breast according to anatomical structure and thermal-physical parameters of tissues, and the heat transfer equation was numerically solved by finite difference method [19].

ANSYS caculation requires that the heat generation rate on volume should be constant normally. However, the heat generation rate of arterial blood perfusion is temperature-dependent and the temperature inside the body is not uniform. This is a nonlinear issue in finite element analysis. In this paper the relationship between heat generation rate of arterial blood perfusion and spatial coordinate inside the body is proposed, based on the characteristic of temperature distribution, and a finite element model of four-layers of human thigh with nonlinear heat generation rate on tissues is established in ANSYS environment. Then a tumor with different sizes and at different depths is taken as the object to investigate the influence of tumor on the temperature distributions inside the body and on the skin surface.

## 2 Theoretical model

The heat transfer in biological tissues was researched by Pennes initially. The mathematical model of bio-heat transfer can be expressed by the partial differential equation of heat conduction:

$$\rho c \frac{\partial T}{\partial t} = \nabla \cdot (k \nabla T) + Q_b + Q_m, \quad (1)$$

$$Q_b = \omega_b \rho_b c_b (T_a - T), \quad (2)$$

Where $\rho$, $c$ and $k$ are the density ($kg/m^3$), specific heat (J/kg·℃) and thermal conductivity (W/m·℃) of tissue, respectively. $\nabla$ represents gradient operator. $Q_b$ is the heat generation rate of arterial blood perfusion ($W/m^3$) and $Q_m$ is the metabolic heat generation rate of tissue ($W/m^3$). $\omega_b$, $\rho_b$, $c_b$ and $T_a$ are the blood perfusion rate (mL/s·$m^3$), blood density ($kg/m^3$), blood specific heat (J/kg·℃) and arterial blood temperature (℃), respectively. At steady state we have $\rho c \frac{\partial T}{\partial t} = 0$. The boundary conditions at skin surface can be described as:

$$q_w = -\vec{n} \cdot (k \nabla T) = h_c (T - T_e), \quad (3)$$

Where $q_w$ is the heat flow ($W/m^2$), $h_c$ is the heat transfer coefficient in the direction of heat flow on the boundary surface due to convection and radiation ($W/m_2$·℃), and $T_e$ is the environmental temperature. In this research $h_c$ and $T_e$ are set to be 13.5 W/($m^2$·℃) and 26 ℃, respectively.

With equations (1) and (3), and by Galerkin method, the integral equation of bio-heat transfer for finite element model can be obtained as follows:

$$\iiint_V \left[ k_x \frac{\partial W_1}{\partial x} \frac{\partial T}{\partial x} + k_y \frac{\partial W_1}{\partial y} \frac{\partial T}{\partial y} + k_z \frac{W_1}{\partial z} \frac{\partial T}{\partial z} - Q_m W_1 - Q_b W_1 + \rho c \frac{\partial T}{\partial t} W_1 \right] dv + \oint_S h_c (T - T_e) W_1 ds = 0, \quad (4)$$

Where $V$ and $S$ are the volume integral and surface integral range, respectively. $W_1$ is the weighting function used in finite element model.

Theoretically speaking, the numerical solution given by finite element analysis can converge to the analytical solution, provided the segmented elements are large enough. In this research the number of grids of meshing is 1.102 millions and the independent test of the meshing is conducted with grid number from 582.5 thousands to 2.586 millions. The experiment results indicate that in this variation range of grids the changes of temperatures at feature point locations are ±0.002 ℃, which is quite satisfactory. There are five steps in the analysis of bio-heat transfer of human body by infinite element model, including establishing geometric model of the body, setting material thermo-physical parameters, meshing, defining heat loads and boundary conditions, solving, and detailed analysis of results under various factors.

## 3 Geometric model and thermo-physical parameters of human thigh

Human thigh can be modeled as an approximate cylinder with four layers of skin, fat, muscle and bone. The thickness and thermo-physical-parameters of each layer are listed in Tab. 1, where the units of the thermo-physical parameters are given in section 1.

**Tab. 1 Thicknesses and thermophysical parameters of tissues**

| | skin | fat | muscle | bone | blood |
|---|---|---|---|---|---|
| Conductivity (W/m·℃) | 0.47 | 0.21 | 0.51 | 0.75 | |
| tissue density(kg/m$^3$) | 1 085 | 920 | 1 085 | 1 357 | 1 059 |
| specific heat(J/kg·℃) | 3 680 | 2 300 | 3 800 | 1 700 | 3 850 |
| Thickness/cm | 0.2 | 0.6 | 2.7 | 2.5 | |
| metabolic heat generate/(W·m$^{-3}$) | 368 | 368 | 684 | 368 | |
| blood perfusion rate(mL/s·m$^3$) | 180 | 180 | 540 | 0 | |

It can be seen from equation (2) that the heat generation rate of blood perfusion is a function of body temperature which is not spatially uniform. This is a nonlinear issue in finite element analysis. The temperature near to skin surface is low and that deep inside the body is much higher. Therefore the heat generation rate of blood perfusion near to skin surface is much higher than that inside the body. M. A. Khanday numerically calculated the temperature distributions of human body along radial direction at various environmental temperatures which were believed to be in good agreement with clinical data [20]. Based on Khanday´s results we propose an equation which gives the heat generation rate of blood perfusion as a function of polar radius instead of body temperature:

$$Q_b = \omega_b \rho_b c_b (kr^n), \quad (5)$$

Where $r$ is the polar radius with length unit of cm, and $k$ and $n$ are undetermined coefficients. The values of $k$ and $n$ should make the value of $kr^n$ almost equal to $(T_a - T)$ with $T$ is the tissue temperature at polar radius of $r$.

According to references of [1] and [21], the tumor doubling time and metabolic heat generation rate are related by a hyperbolic function:

$$Q_m \tau = 3.27 \times 10^6 (\mathrm{W\,day/m^3}), \quad (6)$$

Where $\tau$ is the time required for the tumor to double its volume with the unit of day. The tumor diameter $D$(m) is related to $\tau$ and can be expressed as:

$$D = 0.01 e^{[0.002134(\tau - 50)]}. \quad (7)$$

Equations (6) and (7) can be used to calculate the metabolic heat rate of tumor with certain diameter. It should be pointed out that the metabolic heat rate for tumors with diameter smaller than 1 cm is considered to be the same as that of tumor with diameter of 1 cm [22].

## 4 Simulation results of finite element analysis with ANSYS software

### 4.1 Finite element model of human thigh

With the thermo-physical parameters of tissues listed in Tab. 1 we establish a cylinder model of human thigh with four layers including skin, fat, muscle and bone. The curvature radius and height of the cylinder are 6 cm, 10 cm. The coordinate origin is set at the center of the cylinder, with $Z$ axis along axial direction of the cylinder. The heat generation rate of blood perfusion for each layer is given by equation (5) with appropriate coefficients of $k$ and $n$. The arterial blood temperature and the environmental temperature are set to be 37 ℃ and 26 ℃, respectively, and the heat transfer coefficient $h_c$ on the

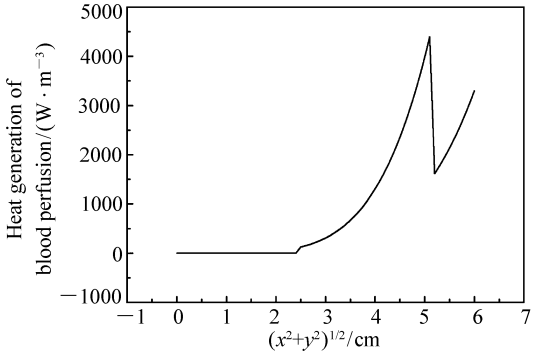


Fig. 1　Distribution of heat generation rate of blood perfusion along radial direction of thigh model

boundary surface is set to be 13.5 W/(m$^2$ · ℃). Fig. 1 is the acquired distribution of heat generation rate of blood perfusion along radial direction in the layers of thigh. It can be seen that the areas of heat generation of blood perfusion include muscle, fat and skin layers, and the muscle layer is the main area of heat generation of blood perfusion. This is because the muscle layer is with the highest blood perfusion rate (three times that of skin layer or fat layer), as well as the biggest thickness (3.4 times that of skin layer plus fat layer).

Fig. 2 shows the temperature distribution at cross-section of thigh model, the plane of $Z$ equal to zero, given by finite element analysis in the case without extra inner heat source. Fig. 2(a) is the color nephogram of temperature distribution and Fig. 2(b) is the variation of temperature along radial direction. It can be seen that the maximum temperature in the body is 37.03 ℃ and the temperature on the skin surface is 32.62 ℃. With the blood perfusion rate, blood density and blood specific heat given by Tab. 1, and the temperature variation date given by Fig. 2(b), we can obtain the curve of heat generation rate of blood perfusion in each layer which is found to be in a good agreement with Fig. 1. This indicates that the methodology used to deal with the nonlinear heat generation rate of artery blood perfusion in this research is suitable.

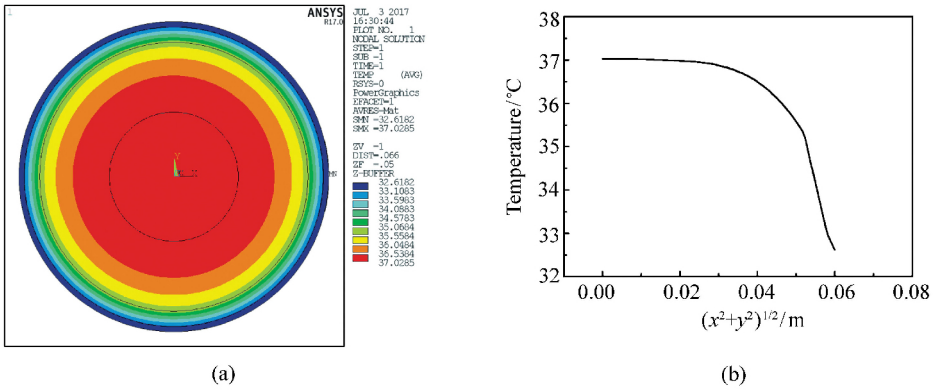


Fig. 2　Temperature distribution at cross-section of the cylinder model with $Z$ equal to zero in the case without extra inner heat source given by finite element analysis. (a) Color nephogram of temperature distribution, and (b) temperature variation along radial direction

### 4.2　Results of finite element analysis for thigh with heat source of a tumor inside

#### 4.2.1　Effects of tumor size

We set a spherical tumor with center position at $X$ axis which is defined as polar axis at plane of $Z$ equal to zero. The variation of $X$ coordinate of the tumor center represents the depth changing along radial direction. For the analysis of the effects of tumor size we set the tumor radius as 0.50 cm, 0.52 cm, 0.55 cm, 0.60 cm and 0.70 cm, respectively. The selection of the range of tumor sizes is due to the following considerations. Firstly, the metabolic heat generation rate for tumors with radius smaller than 0.5 cm is the same as that of tumor with radius of 0.5 cm, and therefore the smaller the tumor size is, the smaller the total metabolic heat

generation. This characteristic is different from that of selected tumors above. Secondly, as the tumor radius larger than 0.70 cm, the larger the tumor size is, the larger the total metabolic heat generation. This characteristic is also different from that of our selected tumors. With equations of (6) and (7) we can get the tumor doubling time and metabolic heat generation rate of the selected tumors. The results are shown in Tab. 2 where the second row lists the tumor doubling time and the third row lists the metabolic heat generation rate of the tumors. It can be seen that as the tumor radius is 0.50 cm the metabolic heat generation rate is 65 400 $W/m^3$, and as the tumor radius increases to 0.55 cm the metabolic heat generation rate drops to 34 544 $W/m^3$ which is 52.82 percent of the former. As the tumor radius further increases to 0.70 cm the metabolic heat generation rate further drops to 15 746 $W/m^3$ which is only 24.08 percent that of tumor with radius of 0.50 cm.

**Tab. 2 Doubling time and metabolic heat generation rate of tumor with different radius**

| $r$/cm | 0.50 | 0.52 | 0.55 | 0.60 | 0.70 |
|---|---|---|---|---|---|
| $\tau$/day | 50 | 68 | 95 | 135 | 208 |
| $Q_m$/(W·m$^{-3}$) | 65 400 | 47 822 | 34 544 | 24 144 | 15 746 |

At first we demonstrate the influence of a tumor on the temperature distribution at cross-section of thigh model by finite element analysis. The radius of the tumor is set to be 0.50 cm and the depth from skin surface to tumor center is set to be 1.4 cm. The simulation results are shown in Fig. 3 where (a) is the color nephogram of temperature distribution at cross-section of the model with $Z$ equal to zero, and (b) is the temperature variation along polar axis($X$ axis). It can be seen that the existence of the tumor results in the temperature distribution changing greatly in the related region. There is a temperature raise in the tumor area with the temperature value as high as 37.66 ℃. In contrast, the temperature at the same spatial position is only 36.22 ℃ in the case without tumor(see Fig. 2).

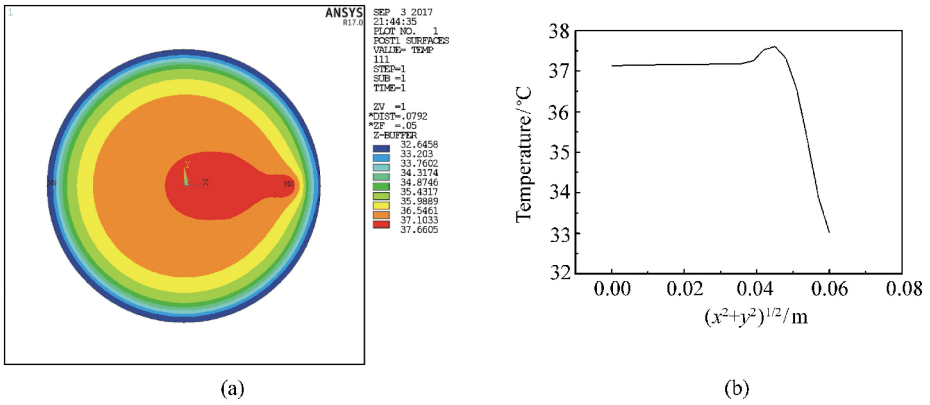


(a) (b)

Fig. 3 Simulation results of temperature distribution at cross-section of cylinder model with a tumor inside by finite element analysis. (a) Color nephogram of temperature distribution at plane of $Z$ equal to zero, and (b) temperature variation along polar axis

Fig. 4 shows the simulation results of the temperature variation along polar axis for different tumor sizes by finite element analysis. The depth from skin surface to tumor center for all tumors is set to be the same of 1.51 cm. It can be seen that the smaller the tumor size is, the higher the temperature raise in the

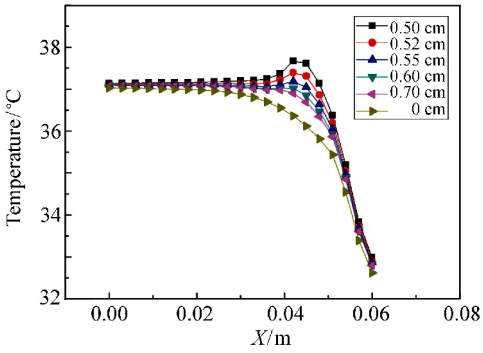


Fig. 4　Finite element analysis results of temperature varying along polar axis for tumors with different radii

related region. The tumor with radius of 0.50 cm yields the highest temperature raise of 1.31 ℃ as compared with the case without tumor, and it is only 0.43 ℃ for the tumor with radius of 0.70 cm. These can be explained as follows. The metabolic heat generation of the tumor is determined by both of the volume and the heat generation rate of the tumor. In the range of the selected sizes of tumors, the heat generation rate plays a more important role, leading to decrease of temperature as increase of tumor size.

Fig. 5 shows the influence of tumor sizes on the temperature distributions on the skin surface where (a) is the temperature distributions along circumference at plane of $Z$ equal to zero, and (b) is the temperature distribution along $Z$ direction. The angle of $\theta$ in Fig. 5(a) is the polar angle with respect to $X$ axis. It can be seen that the variations of the temperature curves with respect to spatial position in Fig. 5(b) are relatively smooth compared with those in Fig. 5(a). However the variation tendency of the curves with respect to tumor size is in good coincidence for Figs. in 5(a) and 5(b). Therefore we discuss the simulation results only with the data in Fig. 5(a). Tab. 3 lists the typical data of the temperature distributions on the skin surface in Fig. 5(a), where the second, third and fourth columns are the maximum, minimum and half maximum of temperature, respectively, and the fifth column is the full width at half maximum of temperature (FWHM) for each curve. The half maximum of temperature is defined as:

$$T_{0.5} = \frac{T_{\max} + T_{\min}}{2}. \tag{8}$$

The FWHM is then defined as the full spatial width of the temperature distribution at the half maximum of temperature.

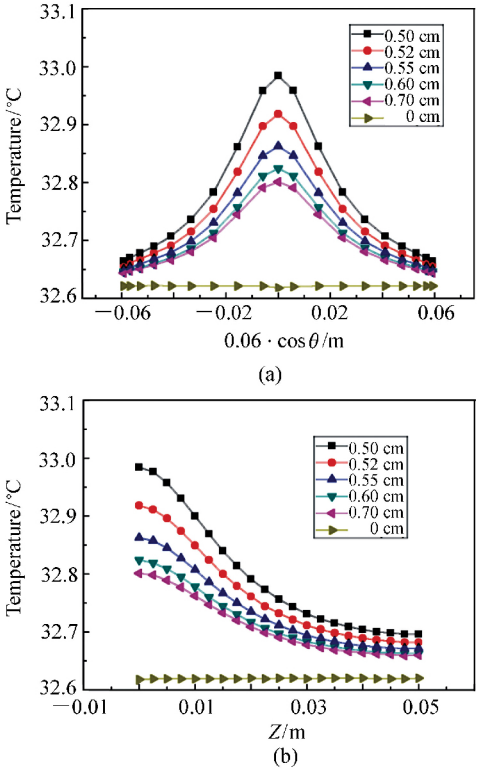


Fig. 5　Temperature distributions on the skin surface for tumors with different sizes inside the model. (a) Temperature distributions along circumference at plane of $Z$ equal to zero, and (b) temperature distributions along $Z$ direction

**Tab. 3　Typical data of the temperature distributions in Fig. 5(a)**

| $r$/cm | $T_{\max}$/℃ | $T_{\min}$/℃ | $T_{0.5}$/℃ | FWHM/cm |
|---|---|---|---|---|
| 0.50 | 32.98 | 32.66 | 32.82 | 4.28 |
| 0.52 | 32.92 | 32.66 | 32.79 | 4.29 |
| 0.55 | 32.86 | 32.65 | 32.76 | 4.31 |
| 0.6 | 32.82 | 32.65 | 32.74 | 4.32 |
| 0.7 | 32.80 | 32.64 | 32.72 | 4.40 |

It can be seen from Fig. 5(a) and Tab. 3 that

the temperature variation with respect to position of skin surface for all curves exhibits a Lorentzian function characteristic. As the radius of tumor increases from 0.50 cm to 0.70 cm, the maximum temperature decreases from 32.98 ℃ to 32.80 ℃. The minimum temperatures for different size of tumors are with small disparity. The minimum temperature is 32.66 ℃ as the tumor radius is 0.50 cm, and it is 32.64 ℃ as the tumor radius is 0.70 cm. Correspondingly, the FWHM of the temperature distribution increases monotonously as the increase of the tumor size. The FWHM is 4.28 cm when the tumor radius is 0.50 cm, and it is 4.40 cm when the tumor radius is 0.70 cm.

4.2.2 Effects of tumor depth

To investigate the effects of tumor depth on the temperature distribution, we set the tumor radius to be 0.50 cm and the range of tumor depths is from 1.4 cm to 2.2 cm with interval of 0.1 cm. Fig. 6 shows the simulation results of the temperature variation along polar axis for different tumor depths by finite element analysis. It can be seen that the existence of tumor causes change in the temperature curve and the bulge point at the position of the tumor

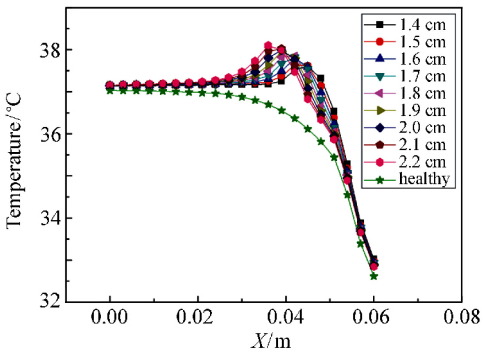


Fig. 6 Finite element analysis results of temperature varying along polar axis for tumors with different depths

center can be observed. The temperature at the bulge point is higher for a tumor located deeper. The temperature is about 38.02 ℃ for the tumor with depth of 2.2 cm, while it is about 37.60 ℃ for the tumor with depth of 1.4 cm. However, little difference of the maximum temperature change with and without tumor can be observed for tumors with different depths. The maximum temperature changes are 1.48 ℃ and 1.44 ℃ for the tumor with center depth of 1.4 cm and 2.2 cm, respectively.

Fig. 7 shows the influence of the tumor depths on the temperature distributions along circumference at plane of $Z$ equal to zero, and along $Z$ direction on the skin surface. It can be seen that the variations of the temperature with spatial position in Fig. 7(b) are relatively smooth as compared with those in Fig. 7(a). However the variation tendency of the curves with respect to tumor depth is in good coincidence in

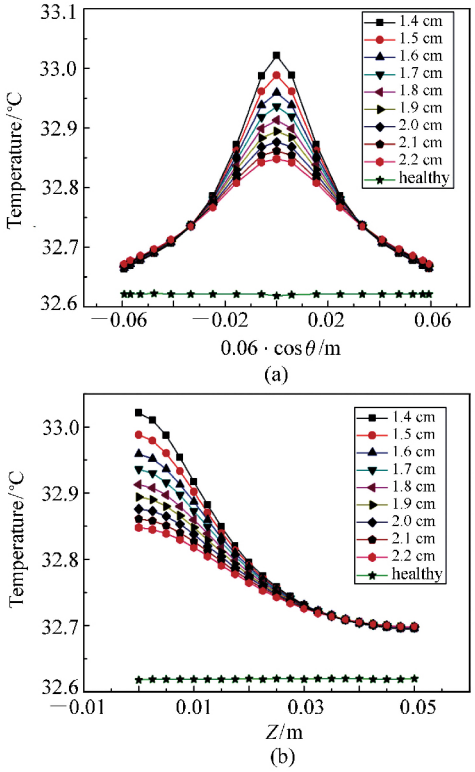


Fig. 7 Temperature distributions on the skin surface for a tumor with different depths inside the model. (a) the temperature distributions along circumference at plane of $Z$ equal to zero, and (b) the temperature distribution along $Z$ direction

Figs. 7(a) and 7(b). Therefore we discuss the simulation results only with the data in Fig. 7(a). Tab. 4 lists the typical data of the temperature distributions on the skin surface in Fig. 7(a), where the

second, third and fourth columns are the maximum, minimum and half maximum of temperature, respectively, and the fifth column is the full width at half maximum of temperature for each curve.

**Tab. 4　Typical data of the temperature distribution curves in Fig. 7( a)**

| $h$/cm | $T_{max}$/℃ | $T_{min}$/℃ | $T_{0.5}$/℃ | FWHM/cm |
|---|---|---|---|---|
| 1.4 | 33.02 | 32.66 | 32.84 | 4.05 |
| 1.5 | 32.99 | 32.66 | 32.83 | 4.26 |
| 1.6 | 32.96 | 32.67 | 32.82 | 4.47 |
| 1.7 | 32.94 | 32.67 | 32.81 | 4.68 |
| 1.8 | 32.91 | 32.67 | 32.79 | 4.89 |
| 1.9 | 32.89 | 32.67 | 32.78 | 5.09 |
| 2.0 | 32.88 | 32.67 | 32.78 | 5.31 |
| 2.1 | 32.86 | 32.67 | 32.77 | 5.54 |
| 2.2 | 32.85 | 32.67 | 32.76 | 5.76 |

It can be seen from Fig. 7( a) and Tab. 4 that the temperature variation with respect to the position of skin surface exhibits a Lorentzian function characteristic. The shallower the tumor depth is, the higher the maximum temperature on the skin surface and the steeper the temperature variation. For the tumor with center at depth of 1.4 cm, the maximum temperature on the skin surface is 33.02 ℃ and the FWHM of temperature is 4.05 cm. For the tumor with center at depth of 1.8 cm, the maximum temperature on the skin surface is 32.91 ℃ and the FWHM of the temperature distribution is 4.89 cm. For the tumor with center at depth of 2.2 cm, the maximum temperature on the skin surface is 32.85 ℃ and the FWHM is 5.76 cm. It can also be seen that although the maximum temperature on the skin surface is of great difference for tumors with different center depths, the minimum temperature is of small difference. The difference of the maximum temperatures is 0.17 ℃ for the tumors with depths of 1.4 cm and 2.2 cm, but the difference of the minimum temperatures is only 0.01 ℃.

### 4.3　Discussion

To evaluate the correction and accuracy of above simulation results, we take A. Chanmugam´s work as comparison. In reference [23] the effects of breast tumor on the surface temperature distribution were presented and were compared with experimental observations using a 3D computational model. It can be seen in Fig. 4 of the reference that for a tumor with fixed radius of 5 mm as the tumor depth decreases from 20 mm to 15 mm, the maximum temperature rise on skin surface increases from 0.08 ℃ to 0.19 ℃. For a comparison, it increases from 0.26 ℃ to 0.37 ℃ in our research. It is noticed that not only the values of temperature rises are in the same order of magnitude as above, but also the increment is the same of 0.11 ℃. For a tumor with fixed depth of 15 mm as tumor radius increases from 5 mm to 7.5 mm, the maximum temperature change on skin surface increases from 0.19 ℃ to 0.50 ℃ in Ref. [23], but decreases from 0.36 ℃ to 0.18 ℃ in our research. Obviously the temperature rises are in the same order of magnitude for both researches, but the variation tendency as tumor size is in contrary. This is because in our simulations the metabolic heat generation rate of tumor as a function of tumor size is taken into account.

## 5　Conclusions

We have established a finite element model of human thigh with four-layers of bone, muscle, fat and skin, and proposed a methodology to solve the nonlinear problem of temperature-dependence of the heat generation rate of blood perfusion in the model. The model is then used to investigate the correlation of the infrared thermal imaging with a tumor inside human body.

It is shown in the given range of tumor diameters that a smaller tumor yields higher temperature raise inside the body, and higher peak temperature and narrower FWHM of the temperature distribution on the skin surface.

It is also shown for tumors at different depths that a tumor located deeper yields higher peak temperature inside the body, and lower peak temperature and wider FWHM of the temperature distribution on the skin surface.

References:


[1] BEZERRA L A, OLIVEIRA M M, ROLIM T L, *et al*.. Estimation of breast tumor thermal properties using infrared images [J]. *Signal Processing*, 2013, 93(10): 2851-2863.

[2] SILVA L F, SANTOS A A S M D, BRAVO R S, *et al*.. Hybrid analysis for indicating patients with breast cancer using temperature time series [J]. *Computer Methods & Programs in Biomedicine*, 2016, 130: 142-153.

[3] SHI G L, HAN F, LIANG C W, *et al*.. A novel method of thermal tomography tumor diagnosis and its clinical practice [J]. *Applied Thermal Engineering*, 2014, 73(1): 408-415.

[4] ETEHADTAVAKOL M, NG E Y K. Breast thermography as a potential non-contact method in the early detection of cancer: a review [J]. *Journal of Mechanics in Medicine & Biology*, 2013, 13(2): 309-107.

[5] XIAO J, HE Z Z, YANG Y, *et al*.. Investigation on three-dimensional temperature field of human knee considering anatomical structure [J]. *International Journal of Heat & Mass Transfer*, 2011, 54(9-10): 1851-1860.

[6] GIUSEPPE C, DANILO E, SUKHOON O, *et al*.. An approach to rapid calculation of temperature change in tissue using spatial filters to approximate effects of thermal conduction [J]. *IEEE Trans. Biomed Eng.*, 2013, 60(6): 1735-1741.

[7] MICHEL A P M, SABBIR L, KEVIN B, *et al*.. In vivo measurement of mid-infrared light scattering from human skin [J]. *Biomedical Optics Express*, 2013, 4(4): 520-530.

[8] BORCHARTT T B, CONCI A, LIMA R C F, *et al*.. Breast thermography from an image processing viewpoint: a survey [J]. *Signal Processing*, 2013, 93(10): 2785-2803.

[9] KENNEDY D A, LEE T, SEELY D. A comparative review of thermography as a breast cancer screening technique [J]. *Integrative Cancer Therapies*, 2009; 8(1): 9-16.

[10] NG Y K. A review of thermography as promising non-invasive detection modality for breast tumor [J]. *International Journal of Thermal Sciences*, 2009, 48(5): 849-859.

[11] PENNES H H. Analysis of tissue and arterial blood temperatures in the resting human forearm [J]. *Journal of Applied Physiology*, 1948, 1(2): 93-122.

[12] BHOWMIK A, REPAKA R. Estimation of growth features and thermophysical properties of melanoma within 3-D human skin using genetic algorithm and simulated annealing [J]. *International Journal of Heat & Mass Transfer*, 2016, 98: 81-95.

[13] DAS K, MISHRA S C. Estimation of tumor characteristics in a breast tissue with known skin surface temperature [J]. *Journal of Thermal Biology*, 2013, 38(6): 311-317.

[14] FERREIRA M S, YANAGIHARA J I. A transient three-dimensional heat transfer model of the human body [J]. *International Communications in Heat & Mass Transfer*, 2009, 36(7): 718-724.

[15] ADLAKHA K R P. Coaxial circular sector elements to study two-dimensional heat distribution problem in dermal regions of human limbs [J]. *Mathematical & Computer Modelling*, 1995, 22(9): 127-140.

[16] AGRAWAL M, PARDASANI K R. Finite element model to study temperature distribution in skin and deep tissues of human limbs [J]. *Journal of Thermal Biology*, 2016, 62(SI): 98-105.

[17] HATWAR R, HERMAN C. Inverse method for quantitative characterization of breast tumors from surface temperature data [J]. *International Journal of Hyperthermia*, 2017, 33(7): 741-757.

[18] WANG C Y, SUN B, CHEN L, *et al*.. Thermal imaging research on relationship between the parameters of the inner abnormal heat source and surface temperature distribution [J]. *Laser & Infrared*, 2012, 42(1): 31-35.

[19] YANG H Q, LIN Q Y, ZHEN Y E, *et al*.. Finite element analysis for temperature distribution of normal breast [J]. *Acta Laser Biology Sinica*, 2007, 16(4): 424-427.

[20] KHANDAY M A. Numerical study of partial differential equations to estimate thermoregulation in human dermal regions

for temperature dependent thermal conductivity [J]. *Journal of the Egyptian Mathematical Society*, 2014, 22(1): 152-155.

[21] MITRA S, BALAJI C. A neural network based estimation of tumor parameters from a breast thermogram [J]. *International Journal of Heat & Mass Transfer*, 2010, 53(21-22): 4714-4727.

[22] NG E Y, SUDHARSAN N M. An improved three-dimensional direct numerical modelling and thermal analysis of a female breast with tumour [J]. *Proceedings of the Institution of Mechanical Engineers Part H Journal of Engineering in Medicine*, 2001, 215(1): 25-37.

[23] CHANMUGAM A, HATWAR R, HERMAN C. Thermal analysis of cancerous breast model [J]. *International Mechanical Engineering Congress and Exposition*, 2012, 2: 134-143.

**作者简介:**

**刘宏岩**(1990—),女,吉林长春人,硕士研究生,2013 年于北京航空航天大学获得学士学位,主要从事红外光学、生物医疗与深度学习方面的研究。E-mail: 270663566@qq.com

**孙　强**(1971—),男,黑龙江海伦人,研究员,2000 年于长春理工大学获得硕士学位,2003 年于南开大学获得博士学位,主要从事红外光学系统设计研究。E-mail: sunq@ciomp.an.cn